

Article

Bartlett–Lewis Model Calibrated with Satellite-Derived Precipitation Data to Estimate Daily Peak 15 Min Rainfall Intensity

Md. Atiqul Islam , Bofu Yu * and Nick Cartwright

School of Engineering and Built Environment, Griffith University, Southport, QLD 4222, Australia; n.cartwright@griffith.edu.au

* Correspondence: atiqul.islam@griffithuni.edu.au (M.A.I.); b.yu@griffith.edu.au (B.Y.)

Abstract: Temporal variability of rainfall is extreme in the rangelands of northern Australia and occurs at annual, decadal, and even longer timescales. To maintain long-term productivity of the rangelands of northern Australia under highly variable rainfall conditions, suitable land management practices are assessed using rangeland biophysical models, e.g., GRASP (GRASs Production). The daily maxima of the 15 min rainfall intensity (I15) are used to predict runoff and moisture retention in the model. The performance of rangeland biophysical models heavily relies on the I15 estimates. As the number of pluviograph stations is very limited in northern Australian rangelands, an empirical I15 model (Fraser) was developed using readily available daily climate variables, i.e., daily rainfall total, daily diurnal temperature range, and daily minimum temperature. The aim of this study is to estimate I15 from daily rainfall totals using a well-established disaggregation scheme coupled with the Bartlett–Lewis rectangular pulse (BLRP) model. In the absence of pluviograph data, the BLRP models (RBL-E and RBL-G) were calibrated with the precipitation statistics estimated using the Integrated Multi-satellitE Retrievals for GPM (global precipitation measurement) (IMERG; 30 min, 0.1° resolution) precipitation product. The Fraser, RBL-E, and RBL-G models were assessed using 1 min pluviograph data at a single test site in Darwin. The results indicated that all three models tended to underestimate the observed I15, while a serious underestimation was observed for RBL-E and RBL-G. The underestimation by the Fraser, RBL-E, and RBL-G models consisted of 23%, 38%, and 50% on average, respectively. Furthermore, the Fraser model represented 29% of the variation in observed I15, whereas RBL-E and RBL-G represented only 7% and 11% of the variation, respectively. A comparison of RBL-E and RBL-G suggested that the difference in the spatial scales of IMERG and pluviograph data needs to be addressed to improve the performance of RBL-E and RBL-G. Overall, the findings of this study demonstrate that the BLRP model calibrated with IMERG statistics has the potential for estimating I15 for the GRASP biophysical model once the scale difference between IMERG and point rainfall data is addressed.



Citation: Islam, M.A.; Yu, B.; Cartwright, N. Bartlett–Lewis Model Calibrated with Satellite-Derived Precipitation Data to Estimate Daily Peak 15 Min Rainfall Intensity. *Atmosphere* **2023**, *14*, 985. <https://doi.org/10.3390/atmos14060985>

Academic Editors: Xiaoming Shi, Berry Wen and Lisa Milani

Received: 8 May 2023

Revised: 2 June 2023

Accepted: 2 June 2023

Published: 6 June 2023

Keywords: rainfall intensity; rangelands; Bartlett–Lewis rectangular pulse model; global precipitation measurement; Integrated Multi-satellitE Retrievals for GPM; Australia

1. Introduction

Interannual variability in rainfall and multi-year wet and dry periods are well-known climatic features in the rangelands of northern Australia [1,2]. As Australian rangelands are mainly used for domestic livestock grazing [3], overgrazing of the pastures (particularly in long drought periods) reduces the plant cover on the soil surface and leads to soil erosion by wind and/or water in wetter periods [4]. Sediments and nutrients eroded from these regions not only increase sediment pollution in downstream river systems and near-shore reefs, but also reduce pasture growth [4,5]. The high variability of rainfall amount and its seasonal distribution impose a major challenge to provide adequate pasture resources for domestic livestock without causing land degradation and affecting pasture recovery [3].



Copyright: © 2023 by the authors. Licensee MDPI, Basel, Switzerland. This article is an open access article distributed under the terms and conditions of the Creative Commons Attribution (CC BY) license (<https://creativecommons.org/licenses/by/4.0/>).

To ensure long-term sustainable productivity of the rangelands of northern Australia, suitable grazing land management practices are developed by simulating the interaction between management practices and degradation processes through the use of the GRASP Production (GRASP) model [6]. The GRASP model consists of linked sub-models (i.e., soil–water balance, pasture, animal, and economic) to mimic the whole system at daily time steps [6]. The soil–water balance sub-model is an important component of the GRASP model, as available soil–water often determines the pasture growth in arid and semi-arid climates [1]. Within the soil–water balance sub-model, surface runoff is estimated using an empirical model derived from the ground cover, daily rainfall, daily maxima of the 15 min rainfall intensity (I15), and soil–water deficit [7]. When the I15 data were missing, a model was developed to estimate I15 values by multiplying the daily rainfall total by a fixed constant for a given Julian day [7].

Although this (Scanlan) model adequately represents the seasonal variation in I15, it needs to be calibrated for a given location against observed I15 data. The requirement of observed I15 data for model calibration considerably limits the application of this model in rangelands in northern Australia as the number of sub-hourly gauge stations is very low in the region. In fact, the spatial and temporal coverage of sub-hourly gauge stations is significantly limited in comparison with the daily gauge stations throughout the country [8].

To overcome this problem, Fraser, et al. [9] developed a model relating I15 to daily rainfall total, diurnal temperature range, and daily minimum temperature. The Fraser model adequately predicts the event size distributions in I15 for a wide range of climates in Australia. Further, the long-term monthly averages of I15 predicted from the model are reasonably close to those of the observed I15 when tested using a dataset derived from 67 Australia-wide pluviograph stations. The most important advantages of the Fraser model are that it does not need to be calibrated against observed I15 data on a site-by-site basis and that the model can be applied at any location in Australia. It is noteworthy that the daily climate data (i.e., rainfall, minimum temperature, and maximum temperature) required for the Fraser model are readily available in Australia [10]. Considering all the above-mentioned facts, the Scanlan I15 model was replaced with the Fraser I15 model in the GRASP biophysical model.

However, the Fraser model accounts for only 46% of the variation in observed I15 and is not suitable to predict individual daily I15 values. It is suitable in biophysical models (e.g., GRASP) only for long-term simulation studies (i.e., 5 years or more). This study aims to overcome this limitation.

In the absence of sub-hourly gauge data, a stochastic rainfall generator (e.g., the Bartlett–Lewis rectangular pulse (BLRP) model) calibrated with satellite-derived precipitation products (SPPs) can be used to generate long rainfall records at sub-hourly timescales. Recently, a disaggregation scheme coupled with the BLRP model was applied to disaggregate daily gauge data into half-hourly time series under different climate conditions of Australia [11]. The Integrated Multi-satellitE Retrievals for GPM (IMERG) precipitation product, derived from the Global Precipitation Measurement (GPM) mission, was used to estimate the BLRP model parameters. Although the BLRP model was calibrated using 30 min IMERG data, it is capable of disaggregating daily gauge data into any finer duration interval less than 30 min.

Traditionally, the BLRP model is calibrated based on the first- to the third-order moments (i.e., the mean, variance, lag-1 auto-covariance, lag-1 auto-correlation, dry proportion, and skewness) of the observed precipitation depths at various sub-daily aggregation intervals (e.g., 5 min to 24 h). The performance of the model is evaluated by comparing the statistics estimated from the generated rainfall time series with those of the observed time series at the aggregation intervals that were used for model calibration (i.e., 5 min to 24 h) [12–14]. To date, only one study has been carried out to simulate rainfall time series at a resolution (e.g., 5 and 15 min) that is finer than that of the input data (e.g., hourly and coarser) [15]. Park, Cross, Onof, Chen and Kim [15] reported that the mean and auto-covariance of rainfall were well reproduced at the sub-hourly timescale (5 and 15 min)

while the variance and skewness were underestimated. Note that the study by Park, Cross, Onof, Chen and Kim [15] used pluviograph data to calibrate the BLRP model parameters. The ability of the BLRP model to reproduce the extremes is validated in the usual way for this class of model by comparing the probability distributions of annual maximum rainfall depths sampled from the observed and generated rainfall time series [12,13]. However, none of the previous studies evaluated the BLRP model in estimating the daily peak rainfall intensity at sub-hourly timescales (e.g., 15 min). Most importantly, no study has been attempted to simulate I15 using the BLRP model fitted with an SPP.

As mentioned above, long-term daily rainfall data are adequate across Australia. Further, the BLRP model fitted with SPPs has not been applied yet to estimate peak rainfall intensity at the sub-hourly timescale. Therefore, this study aims to estimate individual daily I15 values from daily rainfall totals using the above-mentioned disaggregation scheme coupled with the BLRP model. The current study was carried out using 1 min pluviograph and 30 min IMERG data over a period of 18 years from January 2002 to December 2019 at a single test site in Darwin. The site was selected to take into consideration the tropical climate, extreme monsoon rainfall mostly associated with tropical cyclones, and adequate record lengths at both sub-daily and daily timescales. The performances of the BLRP models within the disaggregation scheme to estimate I15 were also compared with the Fraser model at the selected site. It is worth mentioning here that the daily climate data (i.e., rainfall, minimum temperature, and maximum temperature) from this selected site were used during the calibration of Fraser model [9]. This may affect all the statements made about the quality of the Fraser model while comparing the performance of the Fraser model in estimating I15 with those of the BLRP models. However, the comparison can still provide meaningful insight into the relative performances of the two approaches as the data used for the calibration of Fraser model are limited to only 9 years (2002–2010) compared to 18 years (2002–2019) in the current study.

2. Data and Methods

2.1. Pluviograph Data

Darwin Airport (station no. 14015, 130.8925° E, 12.4239° S) is located on the tropical north coast of Australia (see Figure 1a). Darwin experiences summer rainfall with annual rainfall falling mostly over the summer months of November–April, while the dry winter period occurs from May to October. During the study period (January 2002–December 2019), the mean annual rainfall was 1754 mm, with the highest recorded daily rainfall of 343 mm. Pluviograph rainfall data at 1 min intervals were available since 29 November 2001. Missing 1 min data were less than 1% for the period 2002–2019. For this study, 1 min data were aggregated to 15 min and daily totals for model development and validation. The pluviograph data used in this study were collected from the Australian Bureau of Meteorology.

2.2. Satellite-Derived Precipitation Products: IMERG

The IMERG precipitation product uses multi-satellite-based passive microwave (PMW) and infrared (IR) rainfall estimates integrated in space and time using motion vectors derived from the modern-era retrospective analysis for research and applications, version 2 (MERRA-2) reanalysis product [16–18]. The merged PMW-IR estimates are then corrected by monthly gridded gauge-based data. Currently, IMERG data are available from June 2000 to present. The IMERG final run product (Version 06B; hereafter named IMERG) with $0.1^\circ \times 0.1^\circ$ (latitude \times longitude) spatial and 30 min temporal resolutions was used in this study. Figure 1b shows the distribution of the IMERG grids around the selected site. Based on the minimum distance between pixel center and the site location, the IMERG pixel was selected to extract the rainfall data.

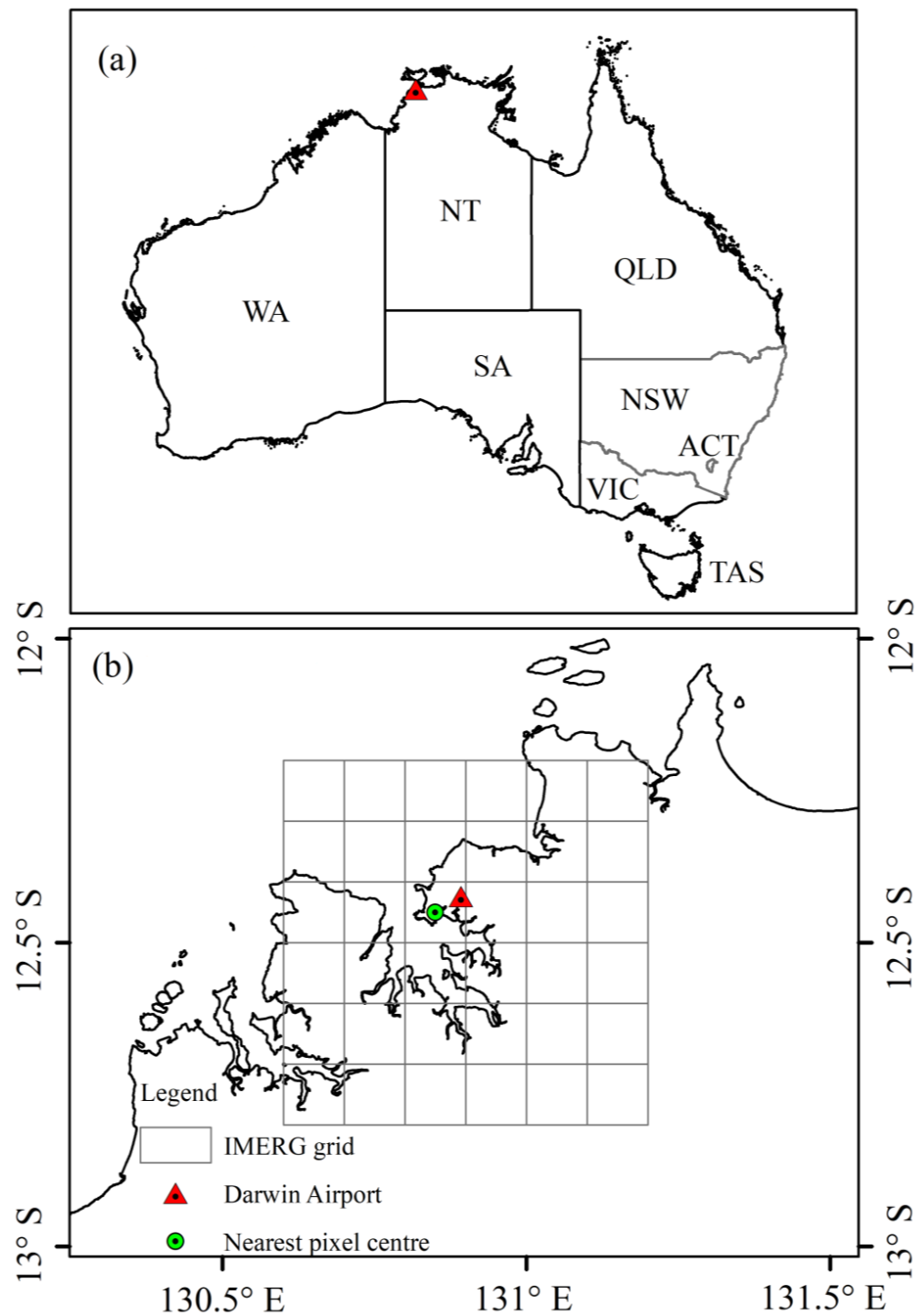


Figure 1. (a) Location of the selected site in Australia and (b) the IMERG grids ($0.1^\circ \times 0.1^\circ$) around the selected site with the nearest pixel center.

2.3. Model Descriptions

2.3.1. Fraser Model

As discussed previously, the I15 model developed by Fraser, Carter, McKeon and Day [9] requires daily minimum temperature, daily diurnal temperature range, and daily rainfall total as the input climate variables. This I15 model was calibrated using the daily

climate variables from 12 selected sites across Australia [9]. According to Fraser, Carter, McKeon and Day [9], the I15 values were estimated using the following equations:

$$I15(a) = \frac{1}{k} \times T_m \times T_r \times \text{minimum}(100, R) \quad (1)$$

$$I15(b) = \begin{cases} I15(a), & \text{if } I15(a) \leq 4 \times R \\ 4 \times R, & \text{if } I15(a) > 4 \times R \end{cases} \quad (2)$$

$$I15 = \begin{cases} I15(b), & \text{if } I15(b) \geq 0.25 \times R \\ 0.25 \times R, & \text{if } I15(b) < 0.25 \times R \end{cases} \quad (3)$$

where T_m is the daily minimum temperature in °C, T_r is the diurnal temperature range in °C, R is the daily rainfall amount in mm, and k (unitless) is the model parameter which was found to be 150 by minimizing the root mean squared error (RMSE) between observed and predicted I15 at the sites. Meanwhile, I15(a) is the daily peak 15 min rainfall intensity in mm/h computed by applying a constraint to the daily rainfall total. If the daily rainfall is greater than 100 mm, it is reduced to the maximum limit of 100 mm (see Equation (1)). This is because the modelled I15 values were not positively correlated with the daily rainfall totals for rainfall amounts greater than 100 mm in a single day. Similarly, I15(b) is the daily peak 15 min rainfall intensity in mm/h and is estimated using an upper limit of the rainfall intensity. If the estimated I15 value is greater than four times the daily rainfall total, the latter is selected as the preferred I15 value (see Equation (2)). Finally, I15 is the daily peak 15 min rainfall intensity in mm/h, which is computed with a lower limit of the intensity. For a particular day, the model selects the maximum one out of the model-derived I15 and one-fourth of the daily rainfall total as the most appropriate I15 value (see Equation (3)).

Note that the Fraser model is applicable only for the days with rainfall amount equal to or greater than 15 mm. The reason is that the daily rainfall less than 15 mm often does not produce a considerable amount of surface runoff in northern Australian rangelands. Further, the Fraser model cannot quantify the amount of uncertainty associated with each I15 value as it is a deterministic model.

2.3.2. Randomized Bartlett–Lewis Rectangular Pulse Model

The BLRP model is a Poisson-cluster-process-based stochastic rainfall generator and simulates storms as clusters of rectangular pulses (rain cells) in time (Figure 2). The original BLRP model proposed by Rodriguez-Iturbe, et al. [19] showed overestimation of the dry periods. To overcome the problem, the original model was modified by randomizing the temporal structure of storms [20]. The randomized Bartlett–Lewis rectangular pulse (RBLRP) model provides greater flexibility to generate different types of storms as well as variability within the storms. A recent version of the RBLRP model developed by Kaczmarek, Isham and Onof [13] was selected in this study to disaggregate the daily pluviograph data. This new version (hereafter named RBLRP_χ) introduces an inverse correlation between rain cell duration and intensity and outperforms other types of BLRP models [12,14,21]. A detailed description of the RBLRP_χ model parameters is given below:

- Storms arrive (solid circles in Figure 2) according to a Poisson process with rate λ [1/T] and each storm is associated with a random number of rain cells.
- Rain cell durations (width of the rectangles in Figure 2) follow the exponential distribution with parameter η [1/T]. The parameter η is allowed to vary from storm to storm following the gamma distribution with shape parameter α (unitless) and scale parameter ν [1/T] and is used to determine the distributions of storm activity time, rain cell arrival, and rain cell depth.
- The storm activity time (solid double arrow lines in Figure 2) is an exponentially distributed random variable with parameter $\eta\phi$, where ϕ (unitless) is a model parameter.
- Rain cells arrive within a storm (open circles in Figure 2) according to a second Poisson process with rate $\eta\kappa$, where κ (unitless) is a model parameter. The origin of the first

rain cell within a storm always coincides with the storm origin. Further, rain cells can arrive only before the termination of the storm activity time.

- The rain cell intensity (height of the rectangles in Figure 2) follows either the exponential distribution with average cell depth η or the gamma distribution with average cell depth η and standard deviation ηr , where ι [T] and r (unitless) are two model parameters.

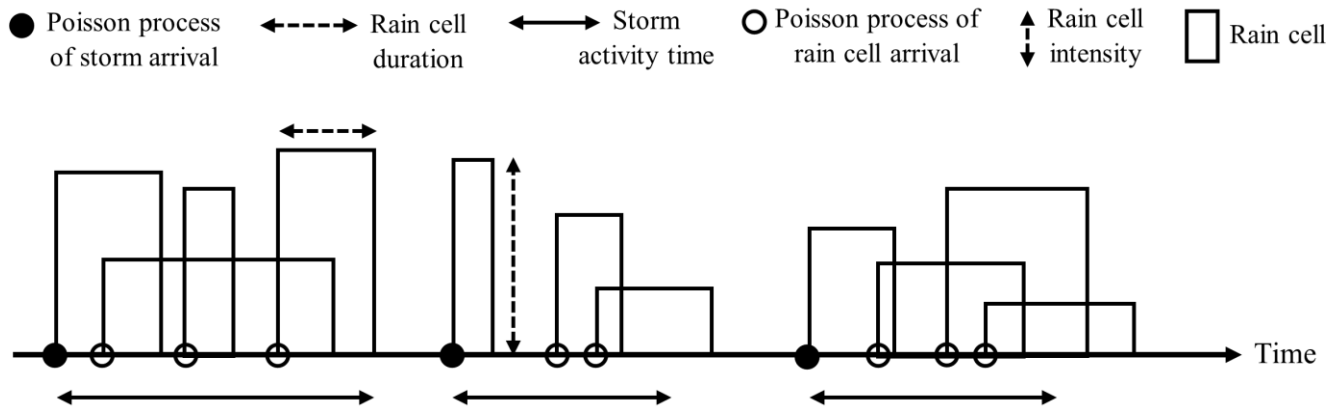


Figure 2. Schematic of the Bartlett–Lewis rectangular pulse model. Note that the model allows overlapping of storms and cells.

Thus, the RBLRP $_{\chi}$ model is characterized by the following seven parameters for the gamma distribution of rain cell intensity: λ [1/T], α (unitless), ν [1/T], κ (unitless), φ (unitless), ι [T], and r (unitless). The exponential distribution is a special case of the gamma distribution when r is equal to 1. Therefore, it is no longer necessary to estimate r for the exponentially distributed rain cell intensity. In practice, the exponential version of the RBLRP $_{\chi}$ model is calibrated with r set to 1.

Model Calibration

The RBLRP $_{\chi}$ model parameters were estimated by minimizing the sum of weighted squared relative departures between the theoretical expressions of the statistics and the corresponding observed values [22]. The theoretical statistics are expressed in terms of the seven parameters [13,20]. The GlobalSearch algorithm [23] was used to calibrate the RBLRP $_{\chi}$ model which minimizes the following objective function:

$$F = \sum_{I=1}^N w_I \left(\frac{\tilde{S}_I}{S_I} - 1 \right)^2 \tag{4}$$

where \tilde{S}_I and S_I are the modelled and observed rainfall statistics, respectively, w_I is the weight assigned to each of the squared relative departures for the selected statistics, and N is the number of statistics selected for use in the calibration and $N = 4$ and 5 in this study. The selected statistics at 0.5 h, 1 h, 2 h, 6 h, 12 h, and 24 h aggregation intervals were included in the objective function. The RBLRP $_{\chi}$ model was calibrated here for both the exponential and gamma distributions of rain cell intensity. For convenience, the models were named depending on the distribution of rain cell intensity and statistics used in the calibration process as follows:

RBL-E: The RBLRP $_{\chi}$ model with the exponentially distributed rain cell intensity that includes the mean, variance, lag-1 auto-covariance, and proportion dry in the parameter estimation.

RBL-G: The RBLRP $_{\chi}$ model with the gamma-distributed rain cell intensity that includes the mean, variance, lag-1 auto-covariance, proportion dry, and skewness in the parameter estimation.

The RBL-G model outperforms the RBL-E model at a site in Bochum, Germany [24]. As the study by Kim and Onof [24] was carried out at a single site, this conclusion cannot be generalized. Thus, both models were selected to enable comparisons in this study. The calibration was performed separately for each calendar month, which produced 12 (monthly) parameter sets for each of the two models. It should be noted that the BLRP models are stationary in time [25]. Only seasonality as a nonstationary feature can be incorporated into the models, which is achieved by fitting the models separately for each calendar month [26].

The selected statistics were computed from IMERG data at the six aggregation intervals (i.e., 0.5 h, 1 h, 2 h, 6 h, 12 h, and 24 h). Having 30 min IMERG, the data at coarser time intervals were obtained via aggregation. Here, the mean, variance, lag-1 auto-covariance, and skewness were estimated from wet periods only, where a wet period was defined as a 30 min rainfall accumulation greater than or equal to 0.2 mm. Because of the biases in IMERG at the 30 min timescale [27], the original 30 min IMERG time series was adjusted with the daily pluviograph data separately for each month to ensure seasonality in the corrected 30 min IMERG data. The corrected 30 min IMERG data were estimated based on the following steps as shown in Figure 3.

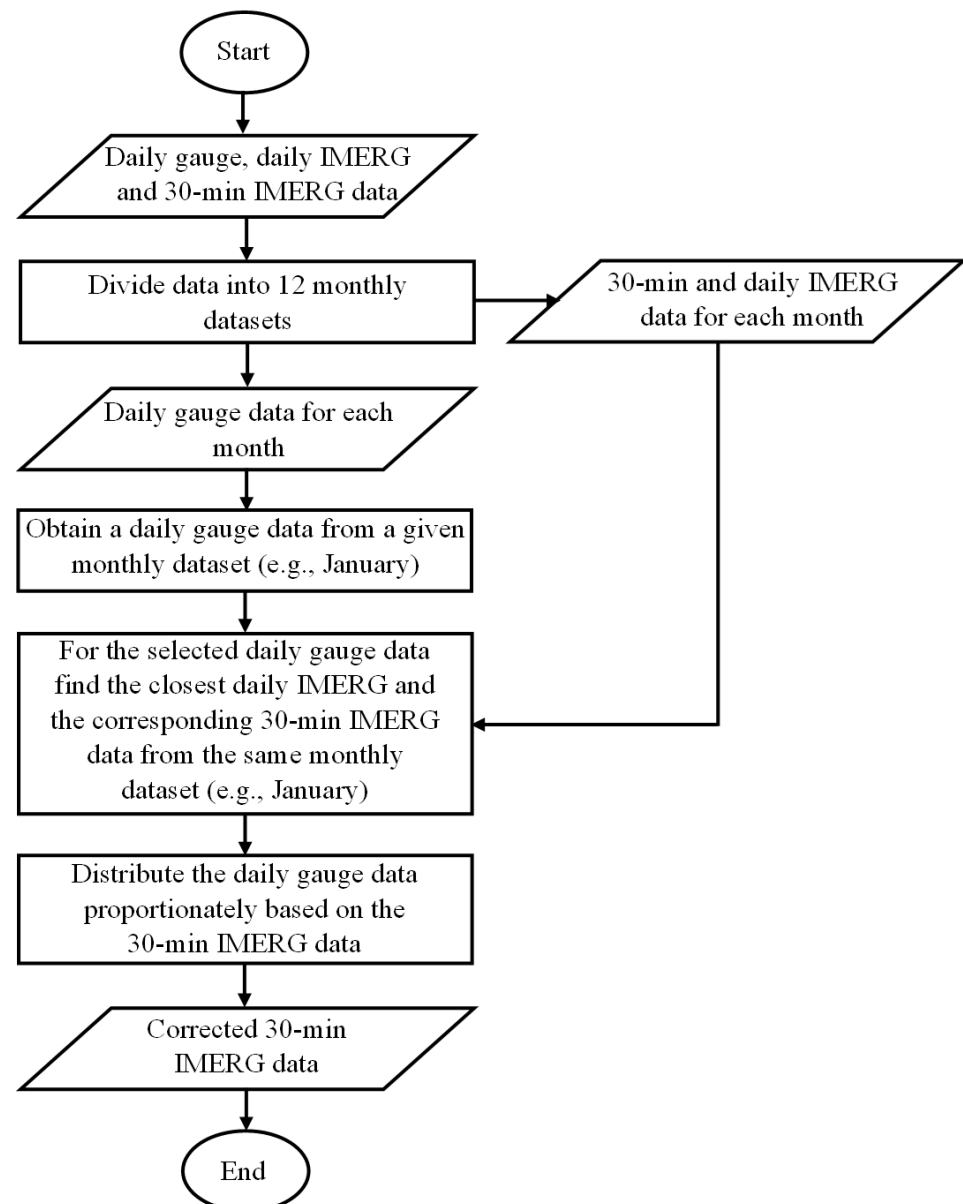


Figure 3. Flowchart illustrating the adjustment of 30 min IMERG data.

Step 1: The 30 min IMERG, daily IMERG (estimated from 30 min IMERG), and daily pluviograph data were divided into different calendar months leading to 12 (monthly) datasets for the entire study period.

Step 2: For a daily pluviograph rainfall total selected from a monthly dataset, the closest daily IMERG and the corresponding 30 min IMERG data were identified from the same monthly dataset.

Step 3: The selected daily pluviograph rainfall total was then proportionally distributed to 30 min time intervals of the day considering the original 30 min IMERG data identified in step 2.

An important note here is that an IMERG pixel represents the average rainfall depth within an area of 10 km × 10 km, whereas a pluviograph measures rainfall at a particular point. The reason to overlook this scale gap here is discussed in Section 3.1.

Disaggregation Scheme

The disaggregation scheme coupled with the BLRP model (i.e., RBL-E or RBL-G) was applied to disaggregate daily pluviograph data into a 15 min rainfall time series based on the following sequences:

- (a) The single- and multi-day wet periods, preceded and followed by one or more dry days, were obtained from the given daily pluviograph time series. The selected BLRP model (i.e., RBL-E or RBL-G) was used to generate storms associated with rain cells for each wet period at the 15 min timescale.
- (b) The intensities of the rain cells were generated for the modelled storms, and the generated daily rainfall depths were calculated to compare with the given daily depths using the following equation [12,28]:

$$d = \left[\sum_{k=1}^L \ln^2 \left(\frac{R_k + c}{\tilde{R}_k + c} \right) \right]^{1/2} \tag{5}$$

where R_k and \tilde{R}_k are the observed and generated rainfall depths in mm, respectively, for the k th day in a wet period of L days. A constant $c = 0.1$ mm was used to avoid domination by the very low daily rainfall values. On the other hand, the logarithmic transformation was selected to prevent domination by the very high rainfall values. For each wet period, the process was repeated until the departure d became lower than an allowable limit d_a . The allowable departure d_a was set to 0.1 as recommended by Kossieris, Makropoulos, Onof and Koutsoyiannis [12].

- (c) According to the proportional adjustment procedure, the generated sub-hourly rainfall depths for the k th day in a wet period of L days were modified as follows [12,28]:

$$X_p = \tilde{X}_p \left(\frac{R_k}{\tilde{R}_k} \right) \quad (p = 1, 2, \dots, \dots, 96) \tag{6}$$

where X_p and \tilde{X}_p are the modified and generated rainfall depths in mm, respectively, for the p th 15 min time interval of the k th day in a wet period of L days.

The disaggregation was performed 100 times to estimate the confidence intervals of the predicted I15 values. In order to assess the disaggregation scheme, rainfall statistics calculated from the disaggregated time series were compared with those of the observed time series at 0.25 h, 0.5 h, 1 h, 2 h, 6 h, 12 h, and 24 h time intervals. In this study, the HyetosMinute R package was used to implement the disaggregation scheme [12,29].

2.4. Performance Criteria

Along with some well-known performance criteria mentioned in Tables 1 and 2, RMSE was used to measure the magnitude of discrepancy between observed and predicted I15 estimates obtained using the Fraser, RBL-E, and RBL-G models. RMSE is dimensional

and has the same unit of measurement as the original observations. RMSE tends to give greater weight to the larger errors and is expressed as follows:

$$RMSE = \sqrt{\frac{1}{n} \sum_{l=1}^n (I15_{m,l} - I15_{o,l})^2} \tag{7}$$

where $I15_{o,l}$ is the l th I15 value estimated from the observed pluviograph data in mm/h, $I15_{m,l}$ is the l th I15 value predicted using the Fraser, RBL-E, or RBL-G models in mm/h, and n is the number of observed or predicted I15 estimates.

Table 1. Regression results for the selected rainfall statistics estimated from original- and corrected-IMERG data ¹.

Parameter	b (SE)		r ²	
	Original IMERG	Corrected IMERG	Original IMERG	Corrected IMERG
Wet-period mean (mm)	0.81 (0.02)	0.93 (0.01)	0.96	0.98
Wet-period variance (mm ²)	0.71 (0.02)	0.97 (0.01)	0.93	0.99
Wet-period lag-1 auto-covariance (mm ²)	0.73 (0.02)	0.96 (0.01)	0.93	0.98
Proportion dry	0.95 (0.01)	0.97 (0.00)	0.97	0.98
Wet-period skewness	1.21 (0.06)	1.17 (0.04)	0.00	0.23

¹ A linear model with zero intercept was used for the five statistics (b: slope for the regression between observed (x) and IMERG (y) statistics estimated from original and corrected data as in $y = bx$; SE: standard error of the estimated slope; r²: correlation coefficient squared).

Table 2. Regression results of the disaggregated rainfall statistics ².

Parameter	b (SE)		r ²	
	RBL-E	RBL-G	RBL-E	RBL-G
Wet-period mean intensity (mm/h)	1.84 (0.10)	1.60 (0.05)	0.70	0.88
Wet-period standard deviation (mm/h)	1.54 (0.09)	1.03 (0.04)	0.69	0.78
Wet-period lag-1 auto-correlation	0.84 (0.10)	1.10 (0.09)	0.31	0.49
Wet-period fraction	0.92 (0.01)	0.90 (0.01)	0.98	0.97
Wet-period skewness	0.84 (0.04)	0.69 (0.04)	0.03	0.00

² A linear model with zero intercept was used for the five statistics (b: slope for the regression between observed (x) and disaggregated (y) rainfall statistics based on RBL-E and RBL-G models as in $y = bx$; SE: standard error of the estimated slope; r²: correlation coefficient squared).

3. Results and Discussion

3.1. Comparison of IMERG with Pluviograph Statistics

The five key rainfall statistics (wet-period mean, wet-period variance, wet-period lag-1 auto-covariance, proportion dry, and wet-period skewness) computed from the original- and corrected-IMERG data were compared with those of the observed data. Figures 4 and 5 show the comparison of the original- and corrected-IMERG data, respectively, at aggregation intervals ranging from 0.5 to 24 h. Linear regression with zero intercept was used to compare the observed statistics to those calculated from original- and corrected-IMERG datasets. Table 1 presents the regression results for the selected rainfall statistics.

As shown in Figure 4a, the original-IMERG dataset generally underestimates the wet-period mean at fine timescales (<6 h). For winter months, the under- and overestimation of the mean are also evident across all timescales. It is interesting to note that the wet-period variance shows a similar pattern to that observed in the wet-period mean, yet the magnitude is different (see Figure 4a,b). In terms of the wet-period lag-1 auto-covariance (Figure 4c,d), the original-IMERG dataset shows a poor correspondence with the observed rainfall data in winter. Despite the overestimation for a few summer months at coarser

timescales (>2 h), the lag-1 auto-covariances estimated from the original-IMERG data are in good agreement with those of the observed data in summer season. Again, the dataset tends to underestimate the dry proportion for summer months across the timescales (see Figure 4e). The wet-period skewness was overestimated most times and showed no clear pattern (see Figure 4f). Note that the skewness values of the original-IMERG data vary over a much wider range than those of the observed data.

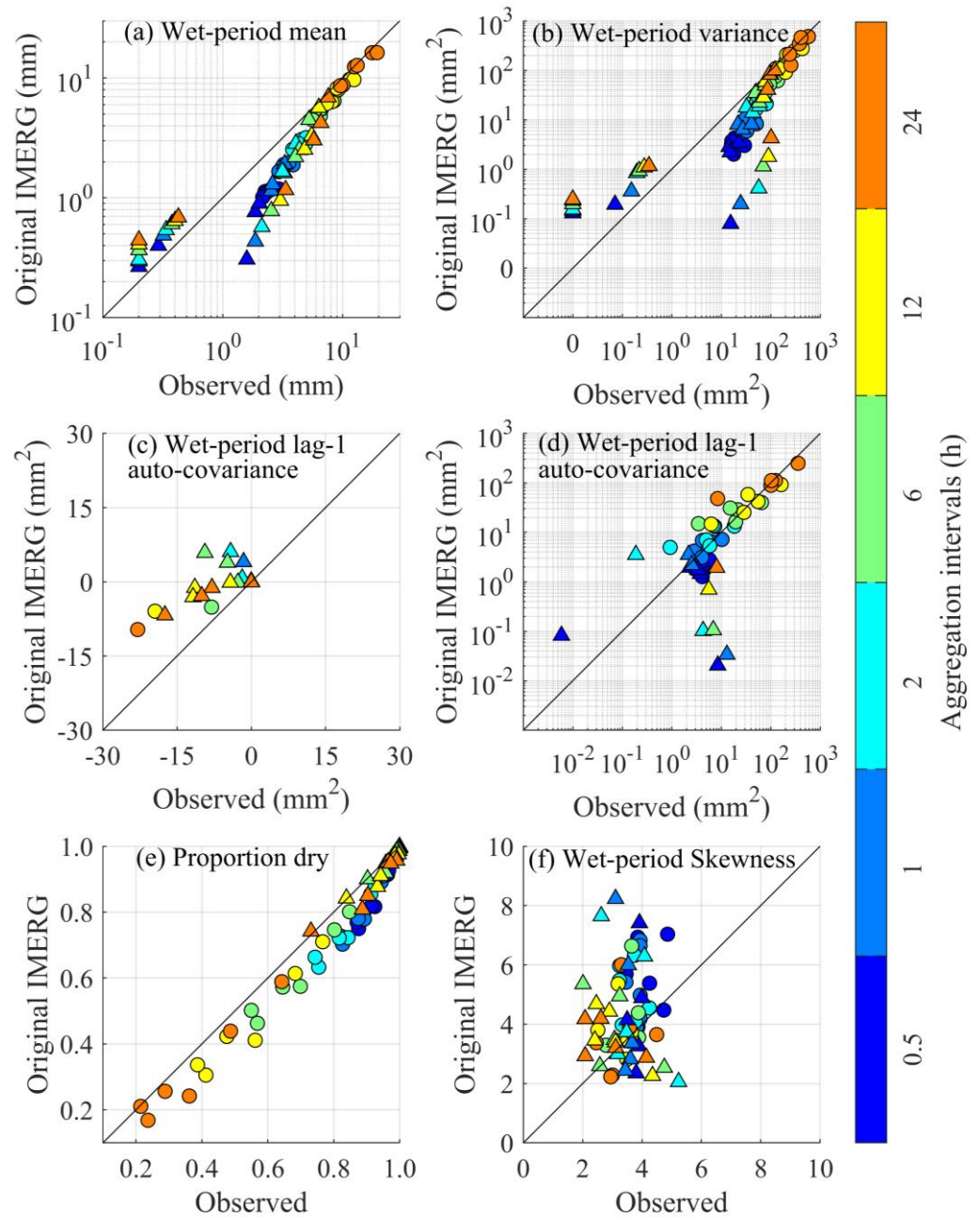


Figure 4. Scatterplots of (a) wet-period mean (mm), (b) wet-period variance (mm²), (c,d) wet-period lag-1 auto-covariance (mm²), (e) proportion dry, and (f) wet-period skewness of the original-IMERG and observed datasets at the six aggregation intervals from 0.5 to 24 h. Panels (c,d) show negative and positive wet-period lag-1 auto-covariances, respectively. The circles and triangles represent the statistics over the summer half of the year (November–April) and winter half, respectively. The face colour of the circles and triangles indicates different aggregation intervals. Each colour has six circles and six triangles representing six months of each season. Note the log–log scale in panels (a,b,d).

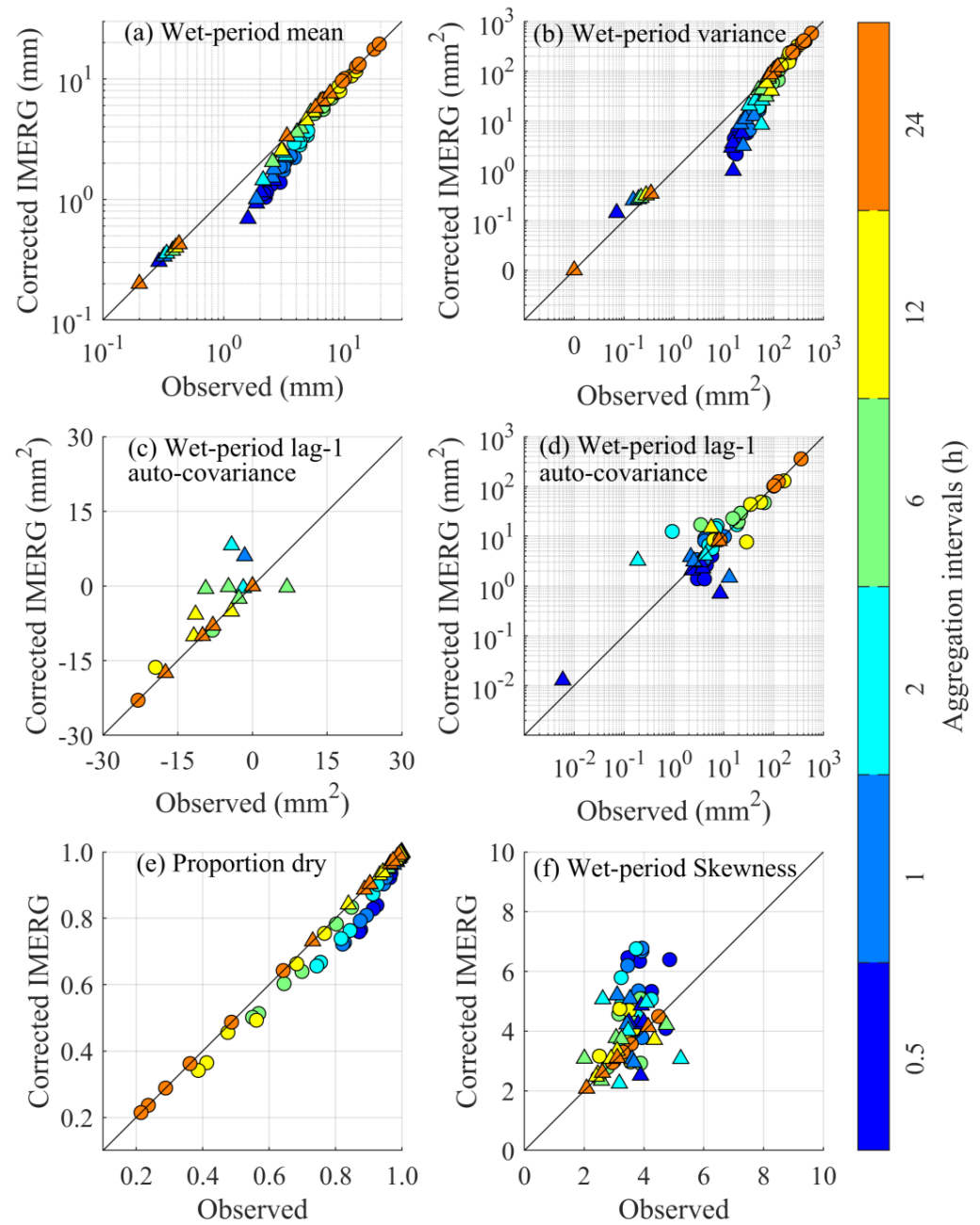


Figure 5. As in Figure 4, but for corrected-IMERG dataset.

The simple bias-correction approach introduced in this study considerably reduces the discrepancy between the IMERG and pluviograph statistics (compare Figure 5 with Figure 4 for the respective statistics and see Table 1). It is seen from Table 1 that all the statistics show an improvement from original- to corrected-IMERG data. In terms of the slope (b), the bias-correction method decreases the overestimation of wet-period skewness by 19% on average for all timescales while reducing the underestimations of other statistics by 63% (wet-period mean), 90% (wet-period variance), 85% (wet-period lag-1 auto-covariance), and 40% (proportion dry). The standard errors (SE) of the corrected-IMERG statistics are lower than those of the original-IMERG statistics. This implies that the adjusted-IMERG statistics are less scattered compared to the original-IMERG statistics. In addition, the corrected-IMERG statistics show better correspondence with the observed statistics than the original-IMERG statistics, as the correlation coefficient squared (r^2) values indicate. Again, the increase in r^2 is relatively high for wet-period skewness out of the five statistics used.

Despite the markedly improved results, there are still some limitations in the corrected-IMERG data, particularly at finer timescales (<6 h). As seen in Figure 5a,b, this dataset underestimates the precipitation mean and variance at fine timescales in both summer and winter seasons. The dry proportion is also underestimated at fine timescales in summer (see Figure 5e). This means that the corrected-IMERG dataset identifies rainfall when in reality there is no rain. Again, the overestimation of skewness is relatively higher for summer months at fine timescales (see Figure 5f). These discrepancies are not ascribed solely to the limitations of the bias-correction method. The underestimation of mean and variance may be attributed to the difference in the spatial scales of IMERG and pluviograph data [30]. An IMERG pixel has an area about 100 km² which is much larger than the sampling area of a pluviograph. The value of an IMERG pixel represents the average rainfall depth within the pixel area, while a pluviograph records rainfall at a particular point. Therefore, even if the IMERG estimate at a pixel is completely accurate, the area-averaged pixel value tends to be smaller than the subpixel point measurements. This issue may result in considerable underestimation in the mean estimated from the original-IMERG data, and consequently from the corrected-IMERG data (see Figures 4a and 5a).

The underestimation of dry proportion may also be partly ascribed to the coarse spatial resolution of IMERG (about 10 km latitude × 10 km longitude). The precipitation systems are mostly convective in summer at the selected site. Short-duration convective storm events often occur over small areas. The coarse-resolution pixel may partly cover the storm area while the collocated pluviograph fails to record any rainfall for being located far from the storm area. The probability of this happening increases as the storm duration becomes shorter. As a result, the dry proportions estimated from the original-IMERG data tend to be underestimated in summer, as observed in Figure 4e. For the summer months, the bias-correction method does well in reducing the underestimation of dry periods at coarser timescales, but is not so good for fine timescales (compare Figure 5e with Figure 4e).

The discrepancy in the spatial scales of IMERG and pluviograph data was not considered here as it is beyond the scope of this paper. It is worth mentioning here that IMERG statistics were not used directly in the RBL-E and RBL-G models and were only applied to determine the model's parameters. Further, the proportional adjustment procedure in the disaggregation scheme confirms that the generated 15 min rainfall time series, when aggregated to daily totals, is identical to the given daily pluviograph record, and overcomes possible under- and overestimation by IMERG with respect to pluviograph measurements (see section Disaggregation scheme). Thus, the proportional adjustment procedure within the disaggregation scheme overrides the bias-correction approach applied in the original-IMERG data at the daily timescale.

3.2. Comparison of Disaggregated with Pluviograph Statistics

The standard precipitation statistics (wet-period mean intensity, wet-period standard deviation, wet-period lag-1 auto-correlation, wet-period fraction, and wet-period skewness) estimated from the observed rainfall time series were compared with those of the disaggregated rainfall time series generated by the RBL-E and RBL-G models. Figures 6 and 7 show the comparison of the RBL-E and RBL-G models, respectively, at timescales varying from 15 min to 24 h. Regression results of the rainfall statistics are presented in Table 2. It should be noted here that statistics at the 15 min timescale were not used in the model calibration and the rainfall time series at coarser timescales (>15 min) were obtained from the 15 min rainfall depths via aggregation.

The prominent feature of Figures 6 and 7 is that both RBL-E and RBL-G models show wider scatters at finer timescales for all the statistics. With respect to b (SE) and r^2 values, the RBL-G model performs better than the RBL-E model to reproduce the wet-period mean intensity, standard deviation, and lag-1 auto-correlation (see Table 2). Meanwhile, RBL-E exhibits a slightly better performance over RBL-G in reproducing the wet-period fraction and skewness. The best values for RBL-G are 1.03 (0.01) and 0.97 for b (SE) and r^2 , respectively, which are obtained for the wet-period standard deviation and wet-period fraction. RBL-E

performs the best for the wet-period fraction with b (SE) of 0.92 (0.01) and r^2 of 0.98. On the other hand, the overestimation of wet-period mean intensity by RBL-E and RBL-G is very significant. In terms of b , RBL-E and RBL-G overestimate the wet-period mean intensity by 84% and 60%, respectively, on average for all the timescales. RBL-E denotes the highest SE value for the wet-period mean intensity and lag-1 auto-correlation, while the SE value of wet-period lag-1 auto-correlation is the highest for RBL-G. Both models also indicate the poorest agreement with the observed wet-period skewness as shown by the lowest r^2 values in Table 2. Overall, the performances of RBL-E and RBL-G models are promising, considering that no sub-daily pluviograph data were used for the model calibration.

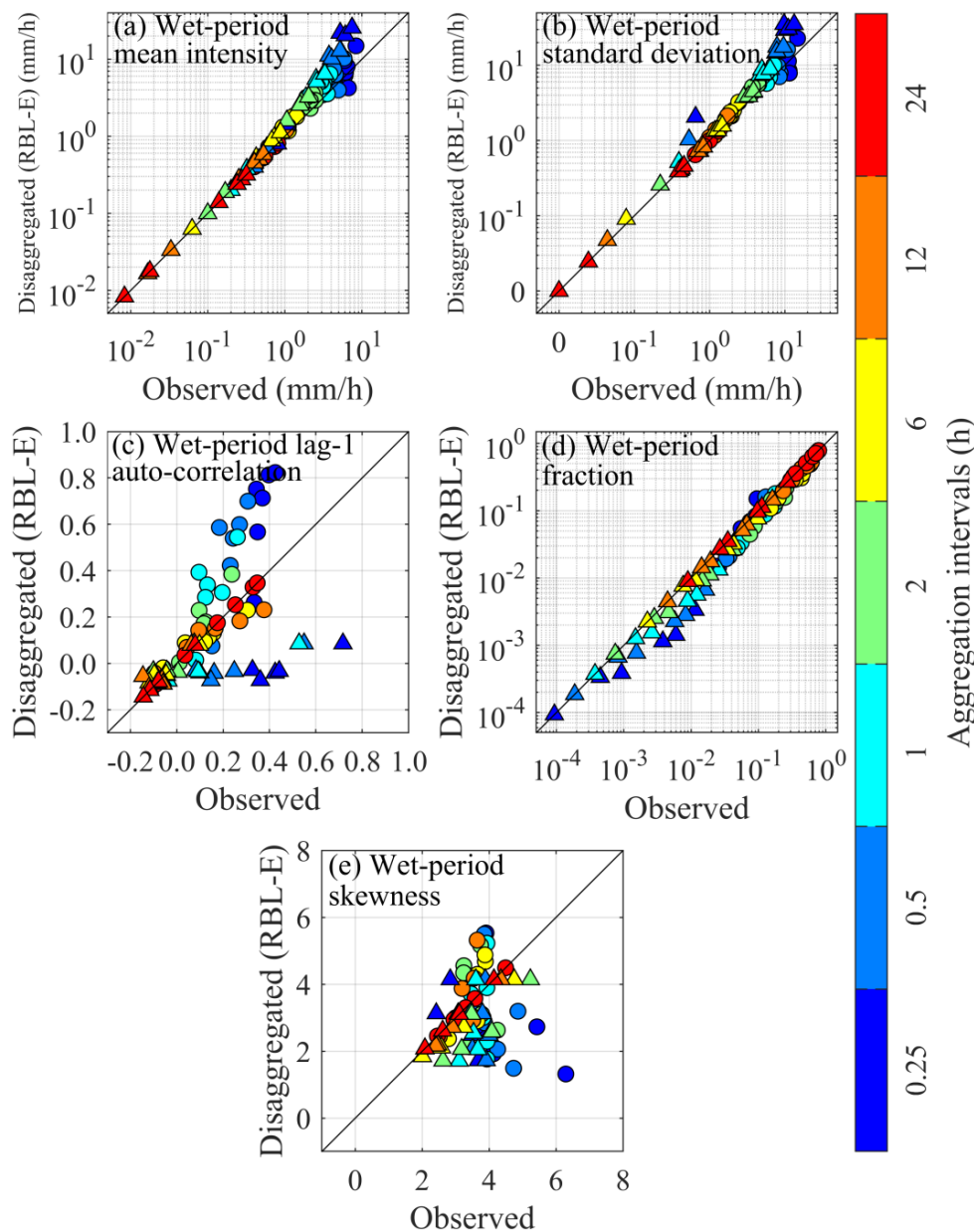


Figure 6. Scatterplots of (a) wet-period mean intensity (mm/h), (b) wet-period standard deviation (mm/h), (c) wet-period lag-1 auto-correlation, (d) wet-period fraction, and (e) wet-period skewness of the disaggregated (RBL-E) and observed datasets at the seven aggregation intervals from 0.25 to 24 h. The circles and triangles represent the statistics over the summer half of the year (November–April) and winter half, respectively. The face colour of the circles and triangles indicates different aggregation intervals. Each colour has six circles and six triangles representing six months of each season. Note the log–log scale in panels (a,b,d).

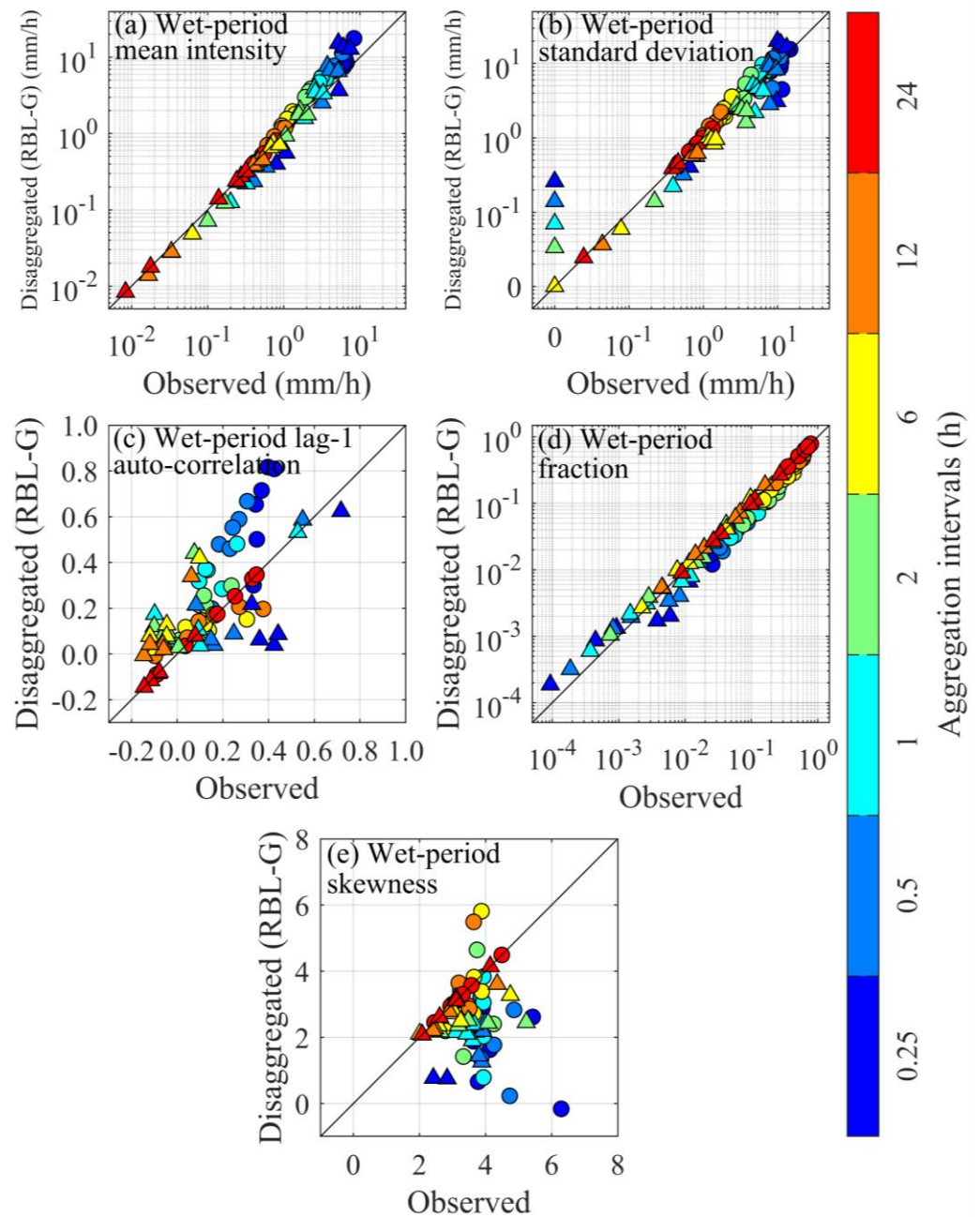


Figure 7. As in Figure 6, but for disaggregated (RBL-G) dataset.

3.3. Comparison of Predicted with Observed I15

To assess the performances of the Fraser, RBL-E, and RBL-G models at the selected site, the model-derived I15 estimates were compared with the observed I15. Scatterplots of the observed versus predicted I15 estimates from the Fraser, RBL-E, and RBL-G models are given in Figure 8. The performance metrics are presented in the upper left corner of each scatterplot. The scatterplots were produced considering days with rainfall equal to or greater than 15 mm, consistent with the Fraser model.

Comparing the scatterplots of the three models, the Fraser model performs relatively better than the median of the RBL-E and RBL-G models. Both RBL-E and RBL-G indicate serious underestimation at higher rainfall intensities (above 20 mm/h), and about 89% of the observed I15 is above 20 mm/h. RBL-E also shows some overestimation at rainfall intensities below 90 mm/h. Comparing the performance metrics of RBL-E and RBL-G, RBL-G appears to be slightly better than RBL-E. The b for RBL-E is better than that of

RBL-G. This is, however, a result of the overestimation at rainfall intensities less than 90 mm/h compensating for the serious underestimation at rainfall intensities greater than 20 mm/h. On going from RBL-E to RBL-G, the underestimation increases from 38% to 50% on average and RMSE decreases from 72% to 65% of the mean of observed I15. A comparison of RBL-G with the Fraser model shows that the Fraser model performs better than RBL-G. The b indicates an improvement from 50% underestimation to 23% on average, and RMSE decreases from 65% to 52%. In terms of SE, RBL-G has less scatter compared to the other two. As shown with the r^2 values in Figure 8, the Fraser model represents 29% of the variation in observed I15, while the corresponding values for RBL-E and RBL-G are only 7% and 11%, respectively.

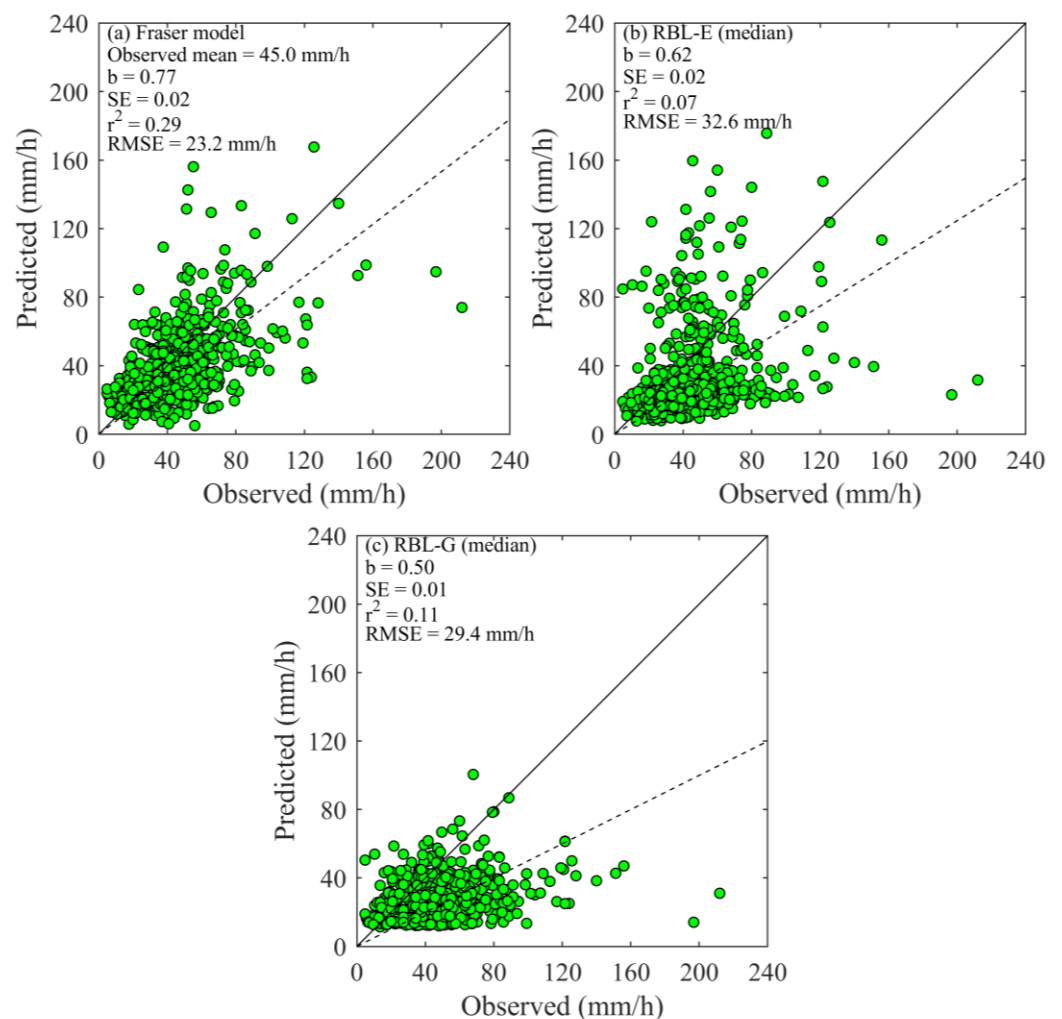


Figure 8. Comparison of the observed and predicted I15 estimates from (a) Fraser, (b) RBL-E, and (c) RBL-G models for the days with rainfall equal to or greater than 15 mm. Performance metrics are shown in the upper left corner of each panel. The solid line shows the 1:1 line, while the dashed line shows the linear regression line between the observed and predicted estimates.

In order to further analyze the performances of the three models, the empirical cumulative distribution functions (ECDFs) of the I15 estimates were compared. In Figure 9, the observed ECDF from the pluviograph data are compared to the ECDFs obtained using the Fraser, RBL-E, and RBL-G models (median and 95% confidence intervals, CI). Each ECDF is based on the ratio of the number of I15 estimates less than or equal to an I15 value (x) to the total number of I15 estimates, $F(x)$, which is plotted against the I15 value (x).

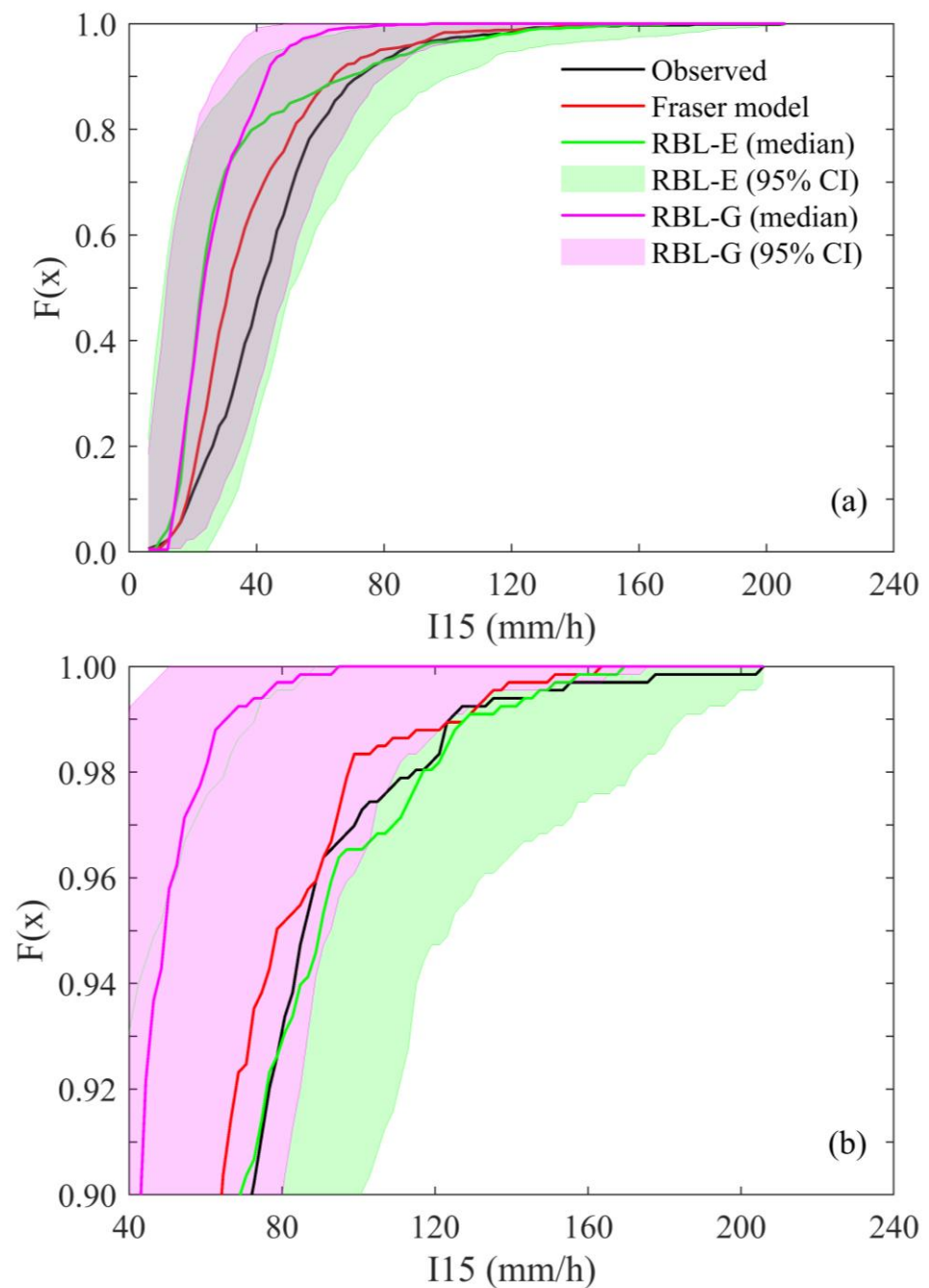


Figure 9. Comparison of the ECDFs of I15 estimates obtained using the Fraser, RBL-E, and RBL-G models with the ECDF of observed I15. The green- and magenta-shaded areas show ECDFs of the 95% confidence intervals (CI) of the I15 values estimated using the RBL-E and RBL-G models, respectively. The panels are drawn considering days with rainfall equal to or greater than 15 mm (a) for 0–240 mm/h and (b) zoomed into the intensity range 40–240 mm/h. On the x-axis, the rainfall intensity is overlapped with different scales on the y-axis.

Comparing the ECDFs, the Fraser model is closer to the pluviograph distribution, while both RBL-E and RBL-G exhibit severe underestimation below 35 mm/h rainfall intensity (see Figure 9a). The significant underestimation by RBL-E decreases with the increase in rainfall intensity (above 35 mm/h), but the large underestimation obtained using the RBL-G model remains even at higher rainfall intensities. This is because, as shown in the scatterplot (see Figure 8c), the range of rainfall intensities is limited for RBL-G (all values are below 101 mm/h). The ECDFs of Fraser and RBL-E models follow the pluviograph

ECDF reasonably well at higher rainfall intensities (see Figure 9b). For RBL-G, 95% of the I15 estimates are below 49 mm/h rainfall intensity, while the corresponding intensities for the Fraser model, RBL-E, and pluviograph are 79, 90, and 86 mm/h, respectively. It can be seen from Figure 9 that the observed ECDF lies within the ECDFs derived from the 95% CI of the RBL-E and RBL-G models, with the exception of the RBL-G model above 107 mm/h rainfall intensity.

The results indicate that none of these models is adequate for estimating I15 values at the selected site. In fact, all the models tend to underestimate the observed I15, with the worst performing models being the RBL-E and RBL-G models. The underestimation of I15 values by RBL-E and RBL-G models may be attributed to the spatial scales of IMERG and pluviograph data. As discussed in Section 3.1, the pixel-based IMERG rainfall estimates tend to be smaller than the collocated pluviograph (point) measurements. Both RBL-E and RBL-G models were calibrated with the statistics (e.g., wet-period mean) estimated from the pixel-based IMERG rainfall estimates. As a result, the I15 estimates obtained using the RBL-E and RBL-G models are likely to be smaller than the pluviograph I15 estimates.

It is worth noting that there are two main differences between RBL-E and RBL-G models (see section Disaggregation scheme). The first is that RBL-E uses the exponential distribution of rain cell intensity, whereas RBL-G assumes the gamma distribution of rain cell intensity. The second difference is that RBL-G includes the wet-period skewness in the model calibration, which is absent from RBL-E. A recent study by Kim and Onof [24] has shown that RBL-G outperforms RBL-E in estimating sub-hourly precipitation extremes at a site in Bochum, Germany. Surprisingly, RBL-G did not show any significant improvement over RBL-E for Darwin in this study. One reason could be the fact that the study by Kim and Onof [24] was carried out at a site located in a temperate climate, as opposed to the tropical climate in Darwin. A comparison of the two models may provide some insight into the relative importance of using the gamma rain cell distribution and skewness in the model calibration versus accounting for the discrepancy in the spatial scales of IMERG and pluviograph data. The results of this study suggest that accounting for the discrepancy in the spatial scales of IMERG and pluviograph data may be more important than using the gamma rain cell distribution and skewness in the calibration process.

4. Summary and Conclusions

According to this study, the statistics estimated from the corrected-IMERG data were relatively closer to the observed statistics than those estimated from the original-IMERG data. The bias-correction approach decreased the overestimation of wet-period skewness by 19% and the underestimation of the wet-period mean, wet-period variance, wet-period lag-1 auto-covariance, and proportion dry by 63%, 90%, 85%, and 40%, respectively. Despite the improvement in the statistics achieved using the simple bias-correction approach, there were noticeable differences between the corrected-IMERG and observed statistics at finer timescales. These differences may partly be ascribed to the difference in the spatial scales of IMERG and pluviograph data.

Comparison of the observed and disaggregated statistics derived from the rainfall time series generated with the RBL-E and RBL-G models showed that the RBL-G model performed better than the RBL-E model in reproducing the wet-period mean intensity, standard deviation, and lag-1 auto-correlation. At the same time, RBL-E was slightly better at reproducing the wet-period fraction and skewness. The best results for RBL-G were associated with the wet-period standard deviation ($b = 0.92$) and wet-period fraction ($SE = 0.01$ and $r^2 = 0.98$), while the performance of RBL-E was found to be the best for the wet-period fraction (b (SE) = 0.92 (0.01) and $r^2 = 0.98$). Conversely, RBL-E and RBL-G overestimated the wet-period mean intensity by 84% and 60%, respectively. RBL-E and RBL-G also performed poorly at reproducing the third-order moment compared to the first- and second-order moments.

The Fraser, RBL-E, and RBL-G models underestimated the observed I15 by 23%, 38%, and 50%, respectively. Further, the Fraser model accounted for 29% of the variation in

observed I15, while RBL-E and RBL-G accounted for only 7% and 11% of the variation, respectively. The large underestimation by RBL-E and RBL-G may partly be associated with the spatial scales of IMERG and pluviograph data. Comparison of RBL-E with RBL-G also suggested that accounting for the difference in the spatial scales of IMERG and pluviograph data may be more important than using different probability distributions for rain cell intensity and skewness of the rainfall time series in the model calibration. Overall, the results of this study highlighted that the RBLRP_χ model fitted with IMERG statistics has the potential for being used as an alternative approach to estimate I15 for the rangeland biophysical model once the scale difference between IMERG and point rainfall data is addressed.

As a consequence of this study, a model could be developed to transform areal rainfall to point rainfall. The transformation of IMERG from an area-averaged to point rainfall could significantly reduce the discrepancy between IMERG and observed statistics, and consequently the underestimation of I15 (e.g., Ombadi et al., 2018). The current research was carried out using precipitation data from a single site located in the tropical climate region. Further research is required to validate the proposed methodology in regions with different climates and precipitation regimes. This could be useful to assess the performance of the proposed methodology in different climates and for different precipitation types. The performance of the BLRP model should also be examined to estimate the I15 when the model is calibrated with the observed pluviograph statistics instead of the IMERG statistics. This is because, to our knowledge, the ability of the observed-statistics-based BLRP model to simulate I15 has not been explored yet. Furthermore, the suitability of other rainfall datasets such as ERA5 (European Centre for Medium-Range Weather Forecasts, ECMWF Reanalysis v5) and GFS (Global Forecast System) to estimate I15 should be explored in future.

Author Contributions: Conceptualization, M.A.I., B.Y. and N.C.; methodology, M.A.I., B.Y. and N.C.; software, M.A.I.; validation, M.A.I.; formal analysis, M.A.I.; investigation, M.A.I.; data curation, M.A.I.; writing—original draft preparation, M.A.I.; writing—review and editing, B.Y. and N.C.; visualization, M.A.I.; supervision, B.Y. and N.C. All authors have read and agreed to the published version of the manuscript.

Funding: This research received no external funding.

Institutional Review Board Statement: Not applicable.

Informed Consent Statement: Not applicable.

Data Availability Statement: Not applicable.

Acknowledgments: The first author acknowledges Griffith University, Queensland, Australia for providing financial support through GUIPRS and GUPRS scholarships. The pluviograph data used in this study were provided by the Commonwealth Bureau of Meteorology. The authors would like to thank Brett Parker of the Griffith Hacky Hour for setting up a Windows machine in the Griffith University HPC Cluster where some analyses were performed.

Conflicts of Interest: The authors declare no conflict of interest.

References

1. Henry, B.; McKeon, G.; Syktus, J.; Carter, J.; Day, K.; Rayner, D. Climate Variability, Climate Change and Land Degradation. *Clim. Land Degrad.* **2007**, *205–221*. [[CrossRef](#)]
2. McKeon, G.; Stone, G.; Ahrens, D.; Carter, J.; Cobon, D.; Irvine, S.; Syktus, J. Queensland's Multi-Year Wet and Dry Periods: Implications for Grazing Enterprises and Pasture Resources. *Rangel. J.* **2021**, *43*, 121–142. [[CrossRef](#)]
3. McKeon, G.M.; Stone, G.S.; Syktus, J.I.; Carter, J.O.; Flood, N.R.; Ahrens, D.G.; Bruget, D.N.; Chilcott, C.R.; Cobon, D.H.; Cowley, R.A.; et al. Climate Change Impacts on Northern Australian Rangeland Livestock Carrying Capacity: A Review of Issues. *Rangel. J.* **2009**, *31*, 1–29. [[CrossRef](#)]
4. McKeon, G.M.; Hall, W.B.; Henry, B.K.; Stone, G.S.; Watson, I.W. *Pasture Degradation and Recovery in Australia's Rangelands: Learning from History*; Queensland Department of Natural Resources, Mines and Energy: Brisbane, Australia, 2004.
5. McKergow, L.A.; Prosser, I.P.; Hughes, A.O.; Brodie, J. Sources of Sediment to the Great Barrier Reef World Heritage Area. *Mar. Pollut. Bull.* **2005**, *51*, 200–211. [[CrossRef](#)]

6. Rickert, K.G.; Stuth, J.W.; McKeon, G.M. Modelling Pasture and Animal Production. In *Field and Laboratory Methods for Grassland and Animal Production Research*; 't Mannetje, L., Jones, R.M., Eds.; CABI Publishing: New York, NY, USA, 2000. [[CrossRef](#)]
7. Scanlan, J.C.; Pressland, A.J.; Myles, D.J. Run-Off and Soil Movement on Mid-Slopes in North-East Queensland Grazed Woodlands. *Rangel. J.* **1996**, *18*, 33–46. [[CrossRef](#)]
8. Green, J.; Johnson, F.; Beesley, C.; The, C. Rainfall Estimation: Design Rainfall. In *Australian Rainfall and Runoff: A Guide to Flood Estimation*; Ball, J., Babister, M., Nathan, R., Weeks, W., Weinmann, E., Retallick, M., Testoni, I., Eds.; Commonwealth of Australia (Geoscience Australia): Barton, ACT, Australia, 2019.
9. Fraser, G.W.; Carter, J.O.; McKeon, G.M.; Day, K.A. A New Empirical Model of Sub-Daily Rainfall Intensity and Its Application in a Rangeland Biophysical Model. *Rangel. J.* **2011**, *33*, 37–48. [[CrossRef](#)]
10. Jeffrey, S.J.; Carter, J.O.; Moodie, K.B.; Beswick, A.R. Using Spatial Interpolation to Construct a Comprehensive Archive of Australian Climate Data. *Environ. Model. Softw.* **2001**, *16*, 309–330. [[CrossRef](#)]
11. Islam, A.; Yu, B.; Cartwright, N. Coupling of Satellite-Derived Precipitation Products with Bartlett-Lewis Model to Estimate Intensity-Frequency-Duration Curves for Remote Areas. *J. Hydrol.* **2022**, *609*, 127743. [[CrossRef](#)]
12. Kossieris, P.; Makropoulos, C.; Onof, C.; Koutsoyiannis, D. A Rainfall Disaggregation Scheme for Sub-Hourly Time Scales: Coupling a Bartlett-Lewis Based Model with Adjusting Procedures. *J. Hydrol.* **2018**, *556*, 980–992. [[CrossRef](#)]
13. Kaczmarek, J.; Isham, V.; Onof, C. Point Process Models for Fine-Resolution Rainfall. *Hydrol. Sci. J.* **2014**, *59*, 1972–1991. [[CrossRef](#)]
14. Cross, D.; Onof, C.; Winter, H.; Bernardara, P. Censored Rainfall Modelling for Estimation of Fine-Scale Extremes. *Hydrol. Earth Syst. Sci.* **2018**, *22*, 727–756. [[CrossRef](#)]
15. Park, J.; Cross, D.; Onof, C.; Chen, Y.; Kim, D. A Simple Scheme to Adjust Poisson Cluster Rectangular Pulse Rainfall Models for Improved Performance at Sub-Hourly Timescales. *J. Hydrol.* **2021**, *598*, 126296. [[CrossRef](#)]
16. Huffman, G.J.; Stocker, E.F.; Bolvin, D.T.; Nelkin, E.J.; Tan, J. *Gpm Imerg Final Precipitation L3 Half Hourly 0.1 Degree X 0.1 Degree V06*; Goddard Earth Sciences Data and Information Services Center (GES DISC): Greenbelt, MD, USA, 2019. [[CrossRef](#)]
17. Huffman, G.J.; Bolvin, D.T.; Braithwaite, D.; Hsu, K.-L.; Joyce, R.J.; Kidd, C.; Nelkin, E.J.; Sorooshian, S.; Stocker, E.F.; Tan, J.; et al. Integrated Multi-Satellite Retrievals for the Global Precipitation Measurement (Gpm) Mission (Imerg). In *Satellite Precipitation Measurement*; Levizzani, V., Kidd, C., Kirschbaum, D.B., Kummerow, C.D., Nakamura, K., Turk, F.K., Eds.; Springer International Publishing: Cham, Switzerland, 2020; pp. 343–353. [[CrossRef](#)]
18. Tan, J.; Huffman, G.J.; Bolvin, D.T.; Nelkin, E.J. Imerg V06: Changes to the Morphing Algorithm. *J. Atmos. Ocean. Technol.* **2019**, *36*, 2471–2482. [[CrossRef](#)]
19. Rodriguez-Iturbe, I.; Cox, D.R.; Isham, V. Some Models for Rainfall Based on Stochastic Point-Processes. *Proc. R. Soc. Lond. Ser. A-Math. Phys. Sci.* **1987**, *410*, 269–288. [[CrossRef](#)]
20. Rodriguez-Iturbe, I.; Cox, D.R.; Isham, V. A Point Process Model for Rainfall—Further Developments. *Proc. R. Soc. Lond. Ser. A-Math. Phys. Sci.* **1988**, *417*, 283–298. [[CrossRef](#)]
21. Onof, C.; Wang, L.-P. Modelling Rainfall with a Bartlett-Lewis Process: New Developments. *Hydrol. Earth Syst. Sci.* **2020**, *24*, 2791–2815. [[CrossRef](#)]
22. Cowpertwait, P.; Isham, V.; Onof, C. Point Process Models of Rainfall: Developments for Fine-Scale Structure. *Proc. R. Soc. A Math. Phys. Eng. Sci.* **2007**, *463*, 2569–2587. [[CrossRef](#)]
23. Ugray, Z.; Lasdon, L.; Plummer, J.; Glover, F.; Kelly, J.; Martí, R. Scatter Search and Local Nlp Solvers: A Multistart Framework for Global Optimization. *INFORMS J. Comput.* **2007**, *19*, 328–340. [[CrossRef](#)]
24. Kim, D.; Onof, C. A Stochastic Rainfall Model That Can Reproduce Important Rainfall Properties across the Timescales from Several Minutes to a Decade. *J. Hydrol.* **2020**, *589*, 125150. [[CrossRef](#)]
25. Wheeler, H.S.; Chandler, R.E.; Onof, C.J.; Isham, V.S.; Bellone, E.; Yang, C.; Lekkas, D.; Lourmas, G.; Segond, M.-L. Spatial-Temporal Rainfall Modelling for Flood Risk Estimation. *Stoch. Environ. Res. Risk Assess.* **2005**, *19*, 403–416. [[CrossRef](#)]
26. Kaczmarek, J.M.; Isham, V.S.; Northrop, P. Local Generalised Method of Moments: An Application to Point Process-Based Rainfall Models. *Environmetrics* **2015**, *26*, 312–325. [[CrossRef](#)]
27. Freitas, E.d.S.; Coelho, V.H.R.; Xuan, Y.; Melo, D.d.C.; Gadelha, A.N.; Santos, E.A.; Galvão, C.d.O.; Filho, G.M.R.; Barbosa, L.R.; Huffman, G.J.; et al. The Performance of the Imerg Satellite-Based Product in Identifying Sub-Daily Rainfall Events and Their Properties. *J. Hydrol.* **2020**, *589*, 125128. [[CrossRef](#)]
28. Koutsoyiannis, D.; Onof, C. Rainfall Disaggregation Using Adjusting Procedures on a Poisson Cluster Model. *J. Hydrol.* **2001**, *246*, 109–122. [[CrossRef](#)]
29. R Core Team. *R: A Language and Environment for Statistical Computing*; R Foundation for Statistical Computing: Vienna, Austria, 2020.
30. Ombadi, M.; Nguyen, P.; Sorooshian, S.; Hsu, K. Developing Intensity-Duration-Frequency (Idf) Curves from Satellite-Based Precipitation: Methodology and Evaluation. *Water Resour. Res.* **2018**, *54*, 7752–7766. [[CrossRef](#)]

Disclaimer/Publisher’s Note: The statements, opinions and data contained in all publications are solely those of the individual author(s) and contributor(s) and not of MDPI and/or the editor(s). MDPI and/or the editor(s) disclaim responsibility for any injury to people or property resulting from any ideas, methods, instructions or products referred to in the content.